EXPERIMENTAL WORKS IN THE NAL HIGH REYNOLDS NUMBER TWO-DIMENSIONAL TRANSONIC WIND TUNNEL ON ADVANCED TECHNOLOGY AND NACA AIRFOILS

Kazuaki Takashima
National Aerospace Laboratory
Chofu, Tokyo, Japan

Abstract

A description of a new wind tunnel at NAL and some results of initial calibration and tests of new transonic airfoils are presented. In order to test the new transonic airfoils at high Reynolds number, a two-dimensional transonic pressure wind tunnel at NAL, Japan was constructed in 1979. This blowdown type wind tunnel has a 0.3 meter wide and 1.0 meter high test section. The performance is 0.2 to 1.15 of Mach number range and 40 x 10^6 of maximum Reynolds number with 10 seconds running time. The wind tunnel starting operation is conducted with precharged air in the tunnel. Closed loop Mach number control is successively applied with excellent regulation and repeatability. Results of the initial calibration indicate adequate performance of the tunnel. The conventional airfoil data are compared with other published experimental results. The Reynolds number effects on the aerodynamic characteristics of NACA 0012 section were experimentally investigated. A few transonic airfoils which were developed at NAL were tested and compared with theoretical and numerical results. Comparisons have been demonstrated good correspondence in some cases as well as gross discrepancies in other cases and those suggest the importance of experimental works.

Symbols

c	chord of airfoil
C_D	section drag coefficient
C_L	section lift coefficient
C_m	section moment coefficient about the 25% chord line
C_N	section normal force coefficient
C_p	pressure coefficient
$C_{p.rms}$	rms value dimensionless broadband pressure fluctuation
M	Mach number
M_S	setting value of Mach number
$\bar{M}$	mean value of Mach number
M_{DD}	drag divergence Mach number
p_0	stagnation pressure
Re	Reynolds number (reference length=c)
T_0	stagnation temperature
x	chordwise station
X_S	shock wave station
α	angle of attack

1. Introduction

In order to provide high Reynolds number testing for the newly developed transonic airfoils, the construction of a two-dimensional transonic pressure wind tunnel at NAL, Japan was commenced in 1973 and completed in fiscal year 1979. The background of the construction of this wind tunnel is explained hereafter.

Since Pearcey[1] announced the concept of a new wing section with peaky pressure distribution in 1960, there has been a strong concentration of interest in transonic wing section development.

One characteristic of such an airfoil is that it has a higher drag rise Mach number or thicker section at the same drag level compared with that of a conventional one. This allows an airplane equipped with such a wing to cruise at higher speed or to be lighter in body and results in higher transportation efficiency or the savings of fuel. Although theoretical and numerical work[2,3,4] on new transonic airfoils is quite active, experimental work is not. We therefore planned to contribute to the development of transonic wing sections through experimental studies.

The other factor in the background of this project was the requirement for high Reynolds number testing especially in the transonic regime. This requirement was noticed in 1960's because the discrepancy between flight test Reynolds number and wind tunnel test Reynolds number was becoming so large that airplane performance prediction by wind tunnel test data was not always satisfactory [5,6]. However, a high Reynolds number test facility for airplane models cannot easily be constructed because of load limitation on the model structure, initial construction cost and energy requirement to operate the facilities. There are many reports on investigation of high Reynolds number test facilities[7,8]. They indicate that high Reynolds number testing can be attained by pressurized and/or cryogenic.

In testing wing sections in a two-dimensional wind tunnel, the difficulties of high Reynolds number testing are reduced by utilizing stout construction of the model support system and a low mass flow rate in the wind tunnel[9,10]. Reynolds number effects on the characteristics of the wing section can be investigated in such a tunnel.

At start of construction of this wind tunnel in 1973, the first oil crisis and the rapid rise of labor costs and material prices were too serious to excute our initial plan. It had to be revised to extend the term of construction. The final budget for this high Reynolds number testing facility was 1,564 million yen.

2. Wind tunnel

Outline[11,12]

The wind tunnel is an intermittent blowdown type. The main parts of this wind tunnel are shown in Figure 1. The height of the central axis of the tunnel is 1.7m from the floor. The outer shell of the plenum chamber is fixed to the basement and the other fixing legs of the wind tunnel are able to slide freely longitudinally to avoid expansion stress due to thermal effects or inner pressure load effects. The basement of the wind tunnel is isolated from the basement of the house to prevent the mutual interaction of vibration through the

basement. An expansion joint is located at the upstream of the pressure regulating valve to separate the wind tunnel from distortion of supply tubes. The strength of the wind tunnel shell of the upstream of the second throat valve was tested at 3041kPa (30kg/cm^{2}G), which is specified by the national control law for high pressure gas.

The principal dimensions are as follows.

Test section	0.3m x 1.0m
Mach number range	0.2 - 1.15
Reynolds number	40 million (M=0.8, c=0.25m)
Stagnation pressure	196 - 1176 kPa
Running time	more than 9 seconds
Maximum mass flow rate	833 kg/sec
Pressure tanks*	2060 kPa
	total volume of 1951 m^3
Compressors*	18000 Nm^3/hour

(* used commonly with other facilities.)
To date, 1800 blows have been conducted.

Pressure regulating valve.

The sleeve-type pressure regulating valve is located upstream from the settling chamber. An axisymmetric, pressure balanced plug is longitudinally moved by a hydraulic cylinder. The outer shell is made of cast steel provided for the complex configuration of the flow path around the plug. In order to reduce pressure loss which occurs near the plug, the flow path surrounding the plug is divided in nine diffusers which are arranged radially as shown in Figure 2. The surface of each diffuser is smoothed during the casting process.

A pilot model of this valve showed favorable performance[13] and it was predicted that the running time would be increased by a factor of about 25 percent compared to it using a conventional valve without diffusers.

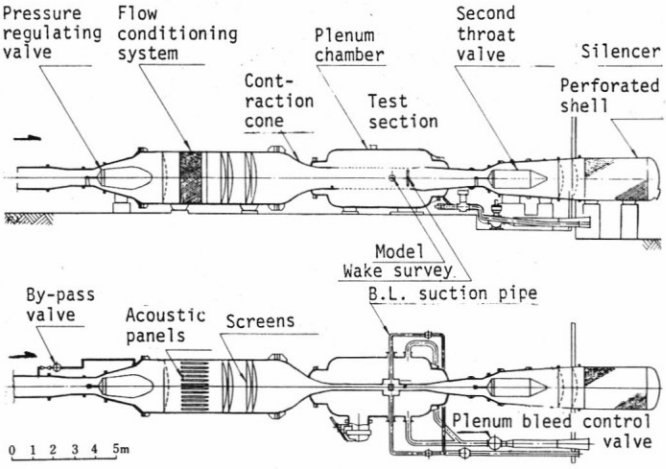

Figure 1. (up)
Schematic diagram of 2-D transonic wind tunnel.

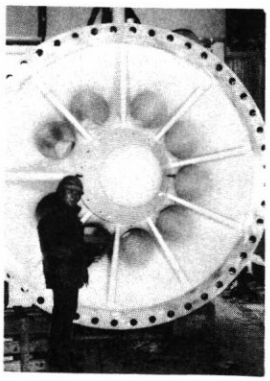

Figure 2. (right)
Downstrem end of pressure regulating valve.

Flow conditioning system (settling chamber).

For the purpose of reducing acoustical noise and eddy turbulence before the air flow reaches the test section, a perforated plate (40% porosity), an acoustical panel array (effective length of 1.0 meter) and four screens (a screen of ten mesh and three of 22.5 mesh) are installed in the settling chamber.

Contraction cone.

The cross section of the flow path is altered from a circle of diameter 2.5m to a rectangular of 1.0m x 0.3m at the 3m long contraction cone. The overall contraction ratio is 16.35:1. The cross sectional area change in the axial direction was calculated based on the one-dimensional theory of Thwaites[14]. After the area distribution was determined, the cross sectional shape was modified with two pairs of straight lines and four circular fairings at the corners, maintaining the same area. The contour coordinates are shown in Figure 3. Preliminary experiments were carried out with a 1/16 scale model[15]. Results indicated the velocity distribution and pressure distribution in the contraction cone model were well predicted by the theory based on one-dimensional flow.

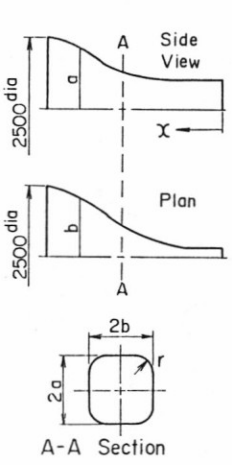

x	a	b	r
0	500.0	150.0	0
200	500.0	154.0	0
400	500.0	162.4	0
600	501.1	180.4	0.8
800	506.7	205.6	12.0
1000	511.7	245.3	44.9
1200	518.8	305.4	106.5
1400	541.2	388.8	200.3
1600	590.6	495.4	325.7
1800	674.5	622.0	478.4
2000	795.4	762.5	650.1
2200	944.9	907.5	828.9
2400	1090.2	1044.8	998.8
2600	1188.1	1159.0	1140.2
2800	1234.6	1231.9	1229.6
3000	1250.0	1250.0	1250.0

(Dimensions in mm.)

Figure 3. Contraction cone.

The test section and the plenum chamber.

The test section is 0.3m wide, 1.0m high and 3.0m long. It is enclosed in the 2.8m diameter plenum chamber. The top and bottom walls are slotted with a variable open-area ratio of zero to ten percent. Six slots are opened in such a way that four slots of the center part have same width and the two slots of the left and right ends have half the width of the center slot.

It is possible for the top and bottom walls to be inclined within ±0.7 degree to the flow axis to reduce the effect of boundary layer development on the walls. After the initial calibration mentioned in Section 3, inclination of those walls was adjusted to a divergence angle of 0.35 degree to maintain uniform Mach number distributions.

The side walls are solid. Near the model support section, the side walls are equipped with either a pair of porous plates or a pair of glass windows depending on the experimental requirement, such as side wall boundary layer control or optical

observation. The porosity of the porous plate, which is made of sintered metal of copper alloy, is the same as that of the hydraulic filter, five micron nominal filtration. Air mass flow which passes through the porous plate is controlled by a ball valve mounted on each suction pipe. The flow is exhausted to the atmosphere through the silencer.

On the right side wall as one faces the upstream, there is a 700mm high by 40mm wide slot downstream from the window for traversing a wake survey probe up and down as shown in Figure 4. A television camera is located at the top and bottom walls to observe the model surface.

The chord length of the wing section model, as shown in Figure 5(a), is usually 250mm. The diameter of the static pressure holes which are opened on the model surface is about 0.6mm. This value is limited by the time lag of pressure leads which is related to the running time. At both ends of the model span, pneumatic connectors are equipped for the pressure leads as shown in Figure 5(b). An O-ring plate is inserted between the model side connector and the mating connector which leads the pressure tubes to the Scani-valve to seal the pneumatic connectors.

A model is of fixed to the model support structures at both ends. Each model support structure is of fixed to a rotating frame which is driven by a hydraulic cylinder, within an angle of -15 to 25 degrees. Model attitude is controlled with a resolution of 0.01 degree. A three component balance which is a powerful device to measure aerodynamic forces acting on the airfoil model has not yet been installed.

The plenum chamber is a pressure vessel which provides a constant static pressure environment for the test section. There is a door of one meter diameter on the left side wall as one faces upstream. A pair of 250mm-diameter x 95mm-thick glass windows are located on each side of the plenum chamber for optical observation. They are removed when the boundary layer suction system is installed at this position. The plenum bleed pipe line, which is located at each side of the plenum chamber, meets the upstream of the plenum bleed control valve that is used for Mach number control above M=0.7. Plenum bleed flow is exhausted to the atmosphere through the silencer.

The second throat valve and diffuser.

The function of the second throat valve, which is located at downstream from the test section, is (i) Mach number control below M=0.75 and (ii) shutting off at precharged start operation which will be explained later.

The diffuser, generally speaking, transforms the kinetic energy of the flow to pressure energy efficiently. In this wind tunnel, however, the high energy flow should be dissipated before atmospheric exhaust. Two perforated plates which are used to dissipate the energy are located in the diffuser. Furthermore, the diffuser is closed by the perforated plate and the downstream shell of the diffuser is also perforated. The pressure loss due to the perforated plate can be estimated by the open-area ratio[13].

Silencer[16].

The silencer is a two storied construction of reinforced concrete, 40m long, 10m wide and 19m high. Air to be discharged from the tunnel enters the first storey. At the end of the air passage in the first storey, the air turns upward and double bents there guide the air into the second storey, which terminates in the form of a stack and discharges the air upward into the atmosphere.

The silencer is enclosed by thick concrete walls everywhere. The upstream section of the first storey is covered by double walls, the inner wall 0.3m and the outer wall 0.2m. Glass wool is attached to the inner surface of the walls and ceilings throughout the first and second storey. Three kinds of acoustic panels are arranged in six arrays in the first storey.

The measured performance is good enough to attenuate the acoustic noise which is generated in a tunnel run. This noise is so insignificant at almost all portions of the NAL site that sound level can not be distinguished from its level at the wind tunnel being quiet.

Instrumentation system.

The instrumentation system consists of sensors, 24 signal conditioners and a data acquisition system which includes an analog-to-digital converter (48 channels, sampling speed of 45 kHz, HP-2313B), a mini-computer (HP-2113B) with 96K-word memory and peripheral equipment. The signals to be measured are basic data for the wind tunnel tests such as the stagnation pressure, angles of attack and so on, the outputs of the pressure transducers which are installed in Scani-valves to obtain pressure distribution on the model surface, the data of wake surveys which are required to get aerodynamic drag and analog signals of miscellaneous channels. In every tunnel run, one to ten pitch attitudes are given to the model in pitch and pause mode and at each pitch attitude, every kind of signal is measured at least one time.

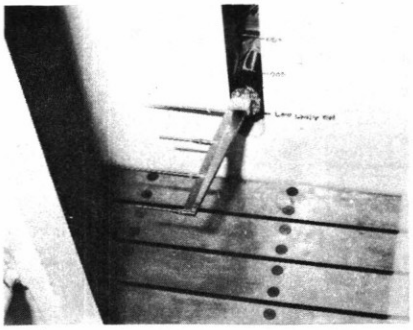

Figure 4. Wake survey probe.

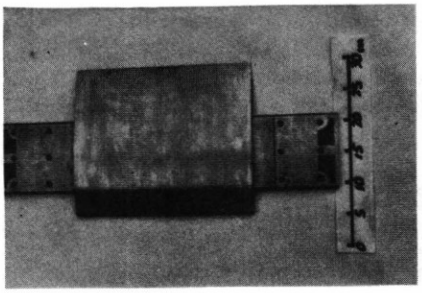

Figure 5(a). Airfoil model.

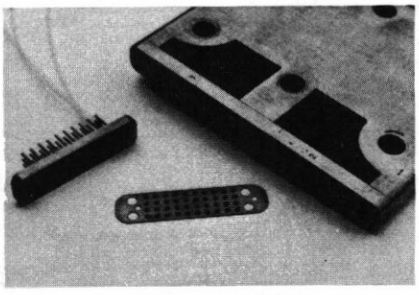

(b). Pressure connector and O-ring plate.

Optical observations can be performed by the schlieren method.

Wind tunnel operating system.

A wind tunnel operating system is available to control required operation automatically by a time schedule programer. The function of this system is (i) one man operation, (ii) accurate setting and regulating, (iii) quick regulation of pressure and Mach numbers and (iv) safe operation for a high pressure wind tunnel. The main features are the starting method and the Mach number control.

Tunnel starting method.

Two ways of start are schemed. One is of course the conventional start of the blowdown wind tunnel. High pressure air is conveyed to the tunnel which is initially at atmospheric pressure. However, if we operate the tunnel this way when a high pressure test condition is required, the large volume of air contained in the settling chamber and the test section is subjected to compression at the initial stage of the start, resulting in adiabatic temperature rise of the flow. During this transient period, the flow condition in the tunnel is not steady. Rapid change of stagnation temperature accompanied by Mach number change is sometimes observed[9].

The second way to start the tunnel, which is suggested by Ohman[9] and is intended by us is that which can be called precharged start. The settling chamber and the test section including the plenum chamber are precharged with air through the bypass valve at a pressure close to the stagnation conditions for the run to follow. In this way we can avoid the trouble mentioned above and expect to lengthen the running time[17].

Closed loop Mach number control.

In order to improve the repeatability of runs and steadiness of the flow in a run, the closed loop Mach number control is available during a run. A pressure ratio of $(p_0-p)/p_0$ is used instead of the Mach number indication which is represented in the more complicated form of p/p_0. The calculation of pressure ratio and the required calculation for the control actions of the second throat valve and/or the plenum bleed control valve are conducted in digital form by a computer which is exclusively used for the tunnel operating system.

3. Results of the initial calibration

To determine the general performance of the wind tunnel, initial calibration was planned to be carried out in three phases. Those were;

Phase 1 measurement at the empty wind tunnel,
Phase 2 measurement of the test section flow in detail and
Phase 3 measurement of the pressure distribution on the typical models.

Those programs were not always conducted in this order. Each program consisted of several subprograms and some subprograms are still continuing.

Measurement at the empty wind tunnel.

The phase 1 program consisted of the confirmation of the Reynolds number and Mach number envelope, measurement of running time, relation of the second throat valve stroke and the plenum bleed control valve openness to the setting Mach number and comparison of the precharged start operation with

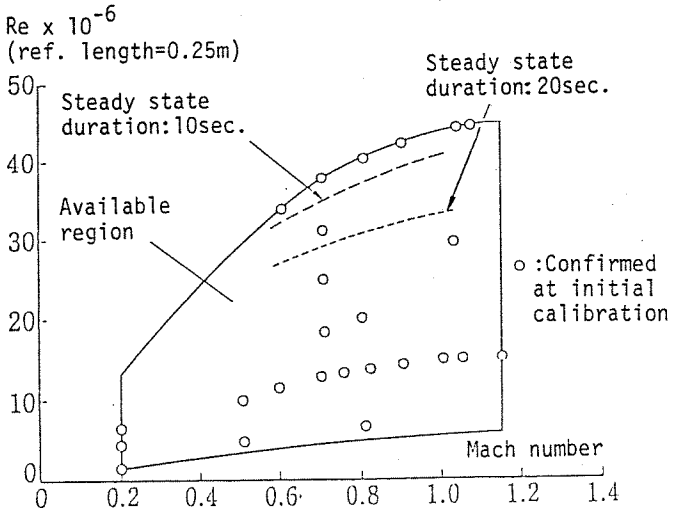

Figure 6. Reynolds number envelope.

the conventional start operation. Results of the phase 1 program showed sufficiently enough to our expectation.

An envelope curve is shown in Figure 6. It indicates that a Reynolds number of 40 million is possible for a 0.25 meter chord model at high subsonic Mach numbers. Usable run times for high Reynolds number tests are enough to measure the physical quantities required.

Comparison between conventional start operation and precharged start operation was conducted about the time histories of the stagnation pressure, Mach number and settling chamber temperature during the starting period. The results are shown in Figure 7. By the application of the precharged start operation, as intended, the flow quantities are moderately changed compared with those obtained in the conventional start operation. Results shown in Figure 7 were obtained at a stagnation pressure of 392 kPa. At the higher stagnation pressure, the conventional start operation did not work well because the pressure difference between screens installed in the settling chamber exceeded the limited value at which the interlock mechanism worked to stop the tunnel for protection of the screens.

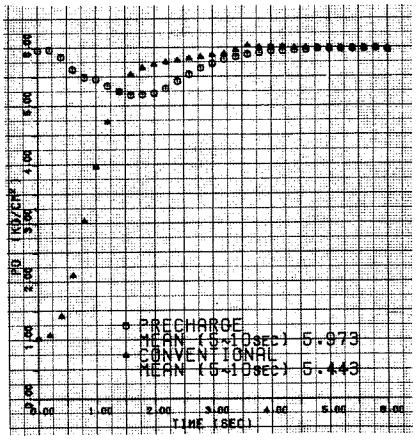

(a) Stagnation pressure.

Figure 7. Comparison of data from precharged start operation and conventional start operation.

(b) Mach number.

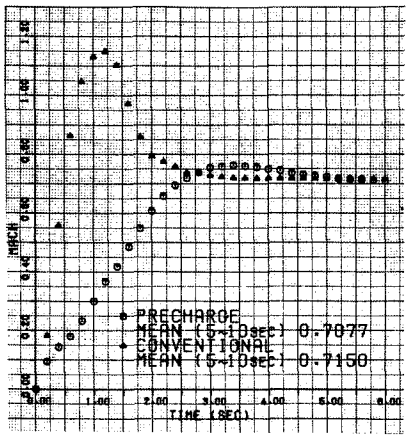

(c) Settling chamber temperature.

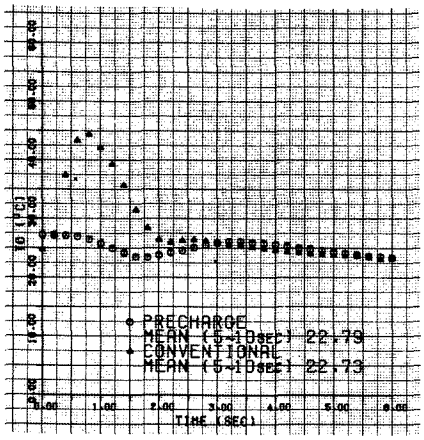

Figure 7. Concluded.

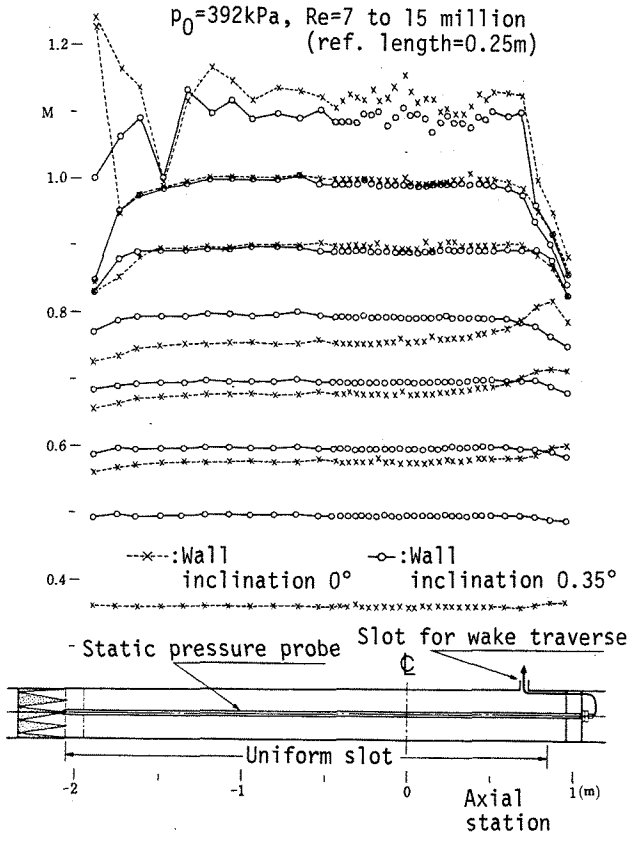

Figure 8. Mach number distribution on the test section center axis.

Measurement of the test section flow.

This program consisted of the measurement of the following quantities. (i) Mach number uniformity, (ii) Flow angularity, (iii) Flow two-dimensionality, (iv) Effect of the side wall boundary layer suction and (v) Flow turbulence level. Items (iii) to (v) have not yet completed; only preliminary studies have been carried out.

For the Mach number uniformity, the static pressure distributions at the test section center axis were measured by making use of a static pressure probe of 3m length. Wall pressure distributions were also measured. Pressure distributions on the center axis are shown in Figure 8. The Mach number uniformity is generally dependent on the wall inclination. After several attempts to discover the best wall inclination, it was found that the best Mach number uniformity was obtained at a wall inclination divergence angle of 0.35 degree for each wall of top and bottom one. At the low supersonic Mach number, uniformity which is shown in Figure 8 is strongly influenced by the static probe support located upstream.

The factor $2\sigma_M$ which represents the index of the Mach number distribution, is within 0.0005 to 0.001 for Mach numbers below 1.0 (where σ_M is standard deviation of the Mach number distribution). So, it is considered that this wind tunnel has excellent Mach number uniformities for the high subsonic region[18].

For the regulation of the Mach number, it was found that the closed loop Mach number control device exhibited excellent performance. The mean value of the Mach number in a run is very close to the setting value of the Mach number which is done by $(p_0-p)/p_0$ setting. Differences of these two values which are shown in Figure 9(a) are less than 0.001. The variation of the Mach number which is occured by the model attitude change is well controlled in a run. The maximum deviation of Mach number from the mean value in a run remains within 0.003 as shown in Figure 9(b).

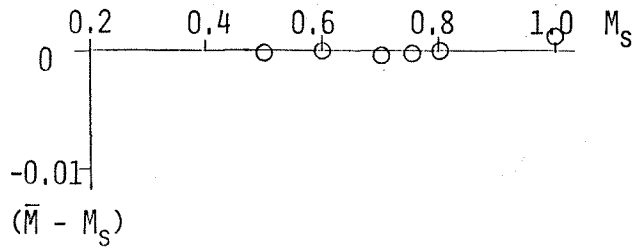

Figure 9(a). Precision of the Mach number setting.

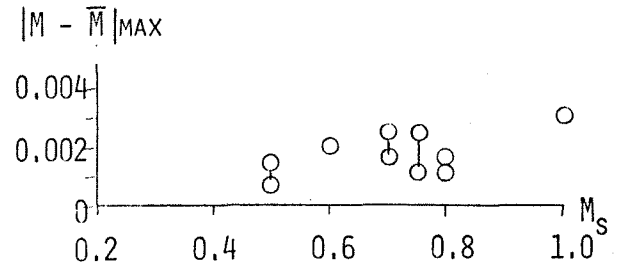

Figure 9(b). Regulation of the Mach number in a run.

Using a symmetrical wing section model (NACA 0012), the flow angularity was measured. In a Mach number range from 0.2 to 0.8, the flow angularity was within $\pm$0.04 degree.

The flow two-dimensionality which was obtained from the pressure distributions on the top and bottom walls was sufficient. For the model, it appears that the flow two-dimensionality of this wind tunnel is at least kept at the middle part of the span for a range of half the span width.

The pressure fluctuation of the flow was measured by means of a microphone-pressure transducer in the test section. Results are shown in Figure 10. The noise of this tunnel is considered moderate. The noise spectrum is studying, compared with those of other wind tunnels[19].

From the investigation of the experimental data mentioned above, it was decided that the plenum chamber pressure would be taken as the reference static pressure which was applied to the free stream Mach number calculation.

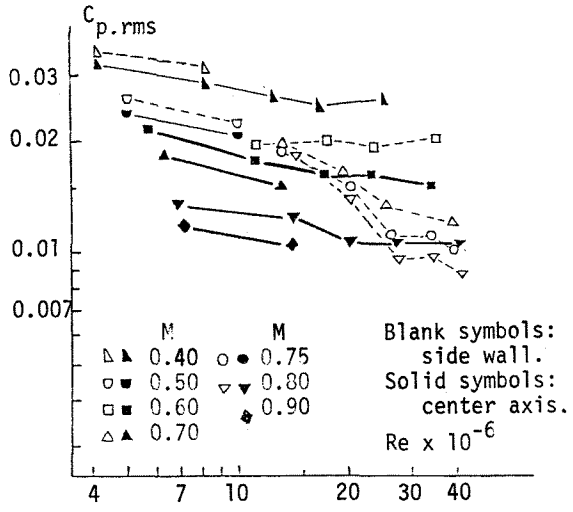

Figure 10. Pressure fluctuation.

Experiments with typical conventional wing sections.

In order to understand the wind tunnel characteristics, pressure distributions for typical wing sections should be compared with those obtained in other wind tunnels. NACA 0012 and 64A410 wing sections were chosen as typical symmetrical and unsymmetrical wing sections, respectively.

All data in this paper are presented in uncorrected form and all tests were conducted for free transition models.

The 64A410 model of chord length 0.25m was tested. The open-area ratio of the slotted wall was set at three percent after some preliminary tests. Pressure distributions at M=0.70, C_N=0.63 which are shown in Figure 11 are compared with those obtained at nearly the same test conditions in NAE high Reynolds number facility[9]. Although as a whole they tend to closely coincide, the discrepancies on the upper surface of x/c=0.2 to 0.4 are presumably caused by the manufacturing error of the models.

Comparison with the numerical results is shown in Figure 12. The numerical results were obtained by the finite difference scheme which was essentially based on the Jameson code[20]. In the numerical calculation, the lift coefficient and Mach number were specified in the same value of experimental data to be compared with. Numerical calculation, especially by non-conservative scheme predicts quite well the shock wave position. The numerical pressure distributions have the same tendency as the experimental one but show a little shift of C_p calues compared with experimental data. The reason for these discrepancies is supposed to be the numerical C_p values near the trailing edge do not agree well with the experimental one and the condition of specifying lift coefficient value which is equal to the experimental value transfers discrepancies to the whole wing section.

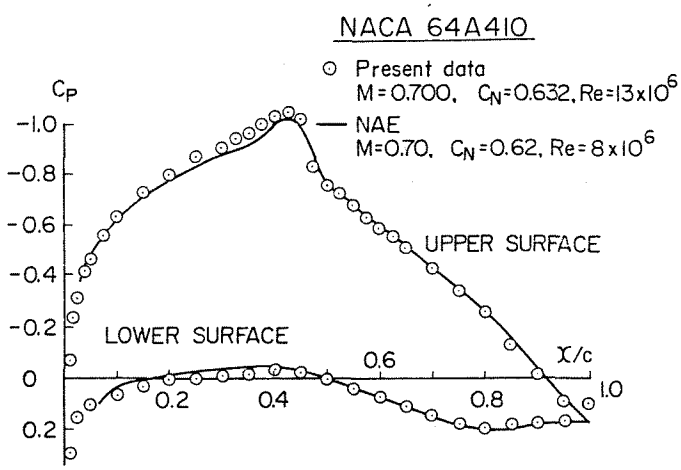

Figure 11. Comparison of pressure distribution data of NAL and NAE.

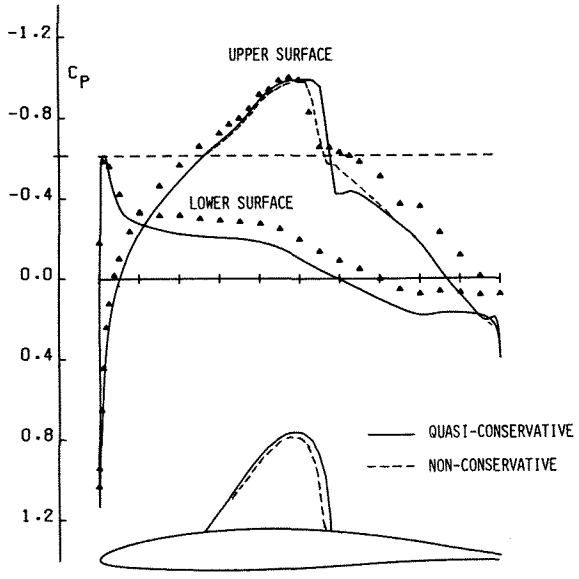

NACA 64A410 M*N=160*30 NCY= 10 R=39 MILLION
THEORY M=.744 ALP=-0.78 CL=0.329 CD=0.0058
△EXPERIMENT M=.744 ALP=-0.01 CL=0.329 CD=0.0091

Figure 12. Comparison of pressure distributions from experiments and calculations.

Aerodynamic coefficients of the lift, drag and pitching moment about a quarter chord of the model are shown in Figure 13. Stivers' results[21] which were obtained at low Reynolds numbers of one tenth are plotted in same figure. Tendency of the present lift coefficient C_L versus Mach number is alike to the Stivers' one at a little smaller level which is presumably caused by wall interference effect.

The pitching moment coefficient of the present data shows great discrepancies from Stivers' one. Generally speaking, Stivers' results show large nose-down moments that increase monotonically with Mach numbers in comparison with present high Reynolds number data. Reynolds number effect on the boundary layer about the airfoil model or wall interference effect is supposedly the origin of this phenomenon. The counter situation which will be described later was observed for the NACA 0012 model.

The NACA 0012 wing section model was tested firstly as a part of initial calibration of the wind tunnel and secondly as an investigation of the Reynolds number effect which will be explained in Section 5.

Pressure distributions at M=0.75, α=4° which are shown in Figure 14 are compared with those obtained from low Reynolds number test at ONERA S3MA wind tunnel[22]. The difference of the shock wave position is thought to be a Reynolds number effect.

Lift and drag coefficients versus Mach number at α=0° and 4° are also shown in Figure 15.

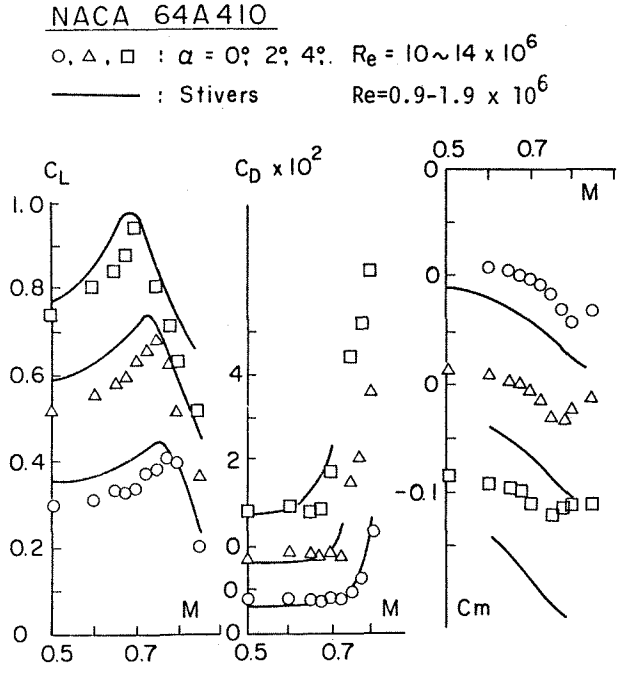

Figure 13. Aerodynamic coefficients of NACA 64A410 wing section.

The effect of the open-area ratio of the slotted wall were investigated with this 0012 model. A typical wall effect on the lift coefficient is clearly observed in the difference of lift curve slopes for the different open-area ratio. After the calculation of the wall correction[23], it is found that this method gives over-correction in this case[24].

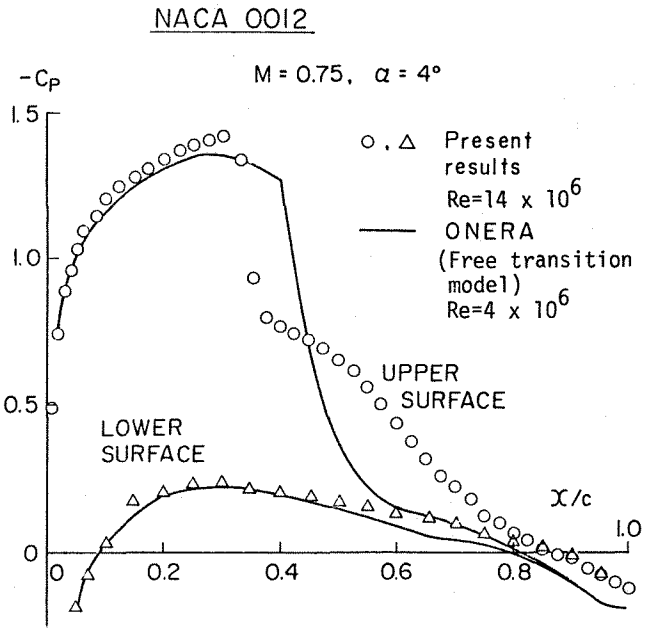

Figure 14. Comparison of pressure distribution data of NAL and ONERA.

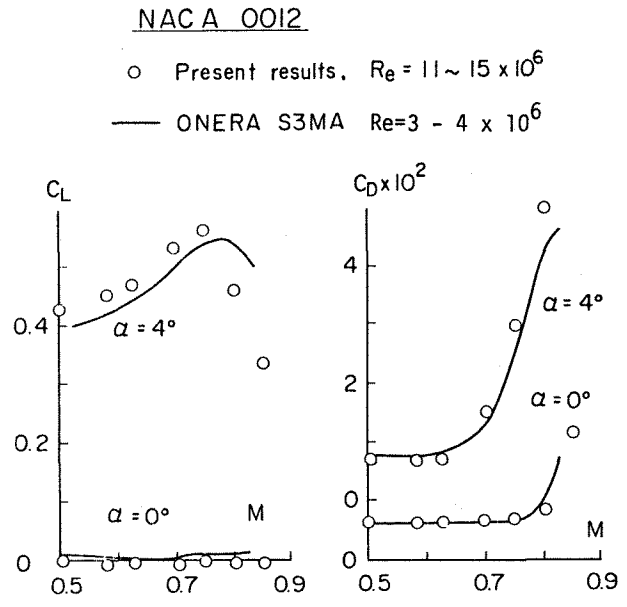

Figure 15. Comparison of aerodynamic coefficients of NAL and ONERA.

4. Results of new wing section models

Shockless wing section of high-C_L.

One of the shockless wing sections which were calculated by the hodograph method developed by our laboratory[25] was tested. A model which was named YM0002 section having an 11% thickness ratio was designed to have a fairly high C_L at a Mach number of near 0.7. The pressure distribution at the design point (M=0.703, C_L=0.945) is shown in Figure 16. A noticeable discrepancy between theoretical prediction and the experimental results is occurence of the shock wave at x/c=0.24.

The shockless pressure distribution was not found at the neighbourhood of the design point for a few Reynolds number cases by the experiment. Presumably, the lift coefficient is, in this case, so large that the experimental pressure distribution does not show the shockless distribution.

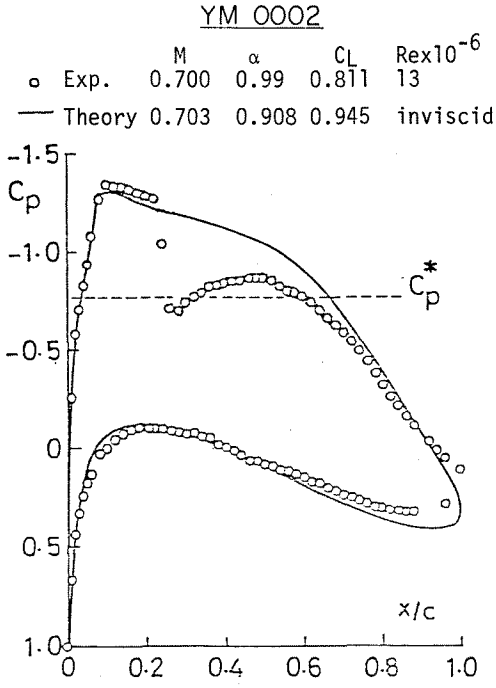

Figure 16. Pressure distributions of NAL YM0002 wing section.

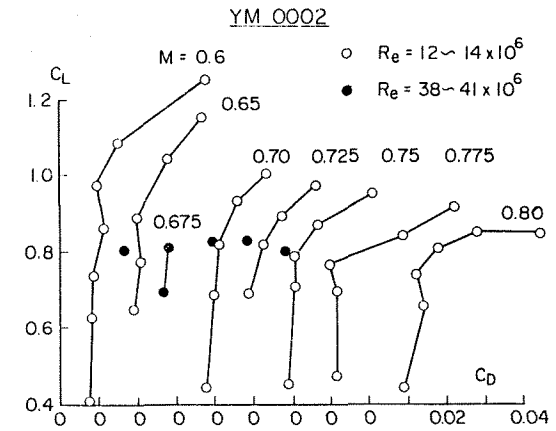

Figure 17. Polar curves of NAL YM0002 wing section.

For the off-design points, the polar curves are shown in Figure 17. A maximum C_L/C_D of about 74 is obtained at M=0.70. The aerodynamic efficiency MC_L/C_D is of about 63 at M=0.65, C_L=0.9 and of 57 at M=0.75, C_L=0.8.

Comparison with the data of the low Reynolds number testing.

A new wing section called 777-626-13, which was designed by subsonic theory[26,27] and investigated with the small wind tunnel (0.1m x 0.4m) with Reynolds numbers of about 2 x 10^6 were tested at moderately high Reynolds number. Results are shown in Figure 18 compared with the data of the low Reynolds number testing. It is recognized that the low Reynolds number testing predicts $(C_L/C_D)_{max}$'s of about 20% less. Leaving the differences of the wind tunnel, the model and the measuring method out of consideration, the discrepancies of the polar curves are significant. The drag divergence Mach numbers which are defined dC_D/dM=0.1 are shown in Figure 19. Although high Reynolds number results are favorable at a region of high C_L's or low M_{DD}'s, those results show an unfaborable trend at low C_L's or high M_{DD}'s. This phenomenon is presumably caused by the movement of the shock wave position due to Reynolds number change and will be discussed in Section 5.

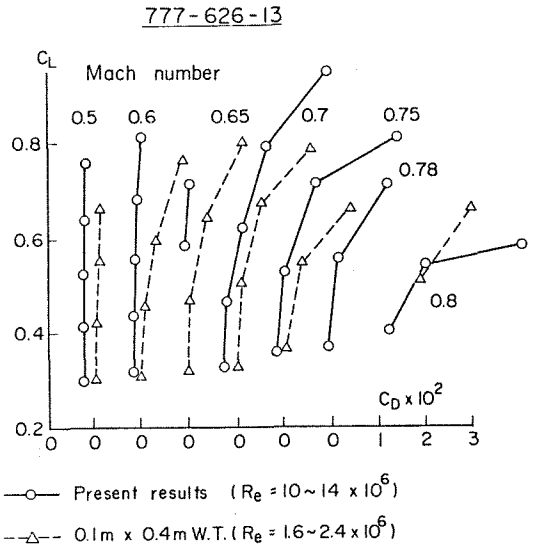

Figure 18. Polar curves of NAL 777-626-13 wing section.

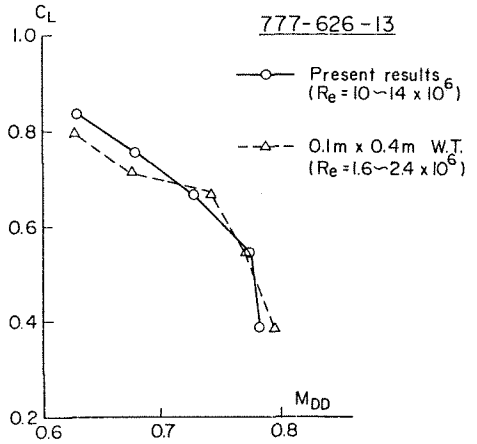

Figure 19. M_{DD} of NAL 777-626-13 wing section.

Verification of the method of wing design by inviscid theory.

A new wing section 75-56-12 which was designed by the relaxation method was tested. Design procedure of this transonic airfoil having specified pressure distribution is owing to Tranen[28] and a computer code which was used was developed by Ishiguro[29]. This code is available in either inviscid or viscous flow design. In this case, design calculation was conducted by inviscid flow of M=0.75 and C_L=0.56. The specified supercritical pressure distributions which have a uniform supersonic region to the chord length of 0.6 and the experimental results of the airfoil model are shown in Figure 20. The pressure distributions on the lower surface agreed well; however those on the upper surface show a significant difference for both the C_p level at the supersonic region and the shock wave position. These discrepancies can surely be improved by design utilizing the viscous flow calculation. The polar curves for a range of M=0.5 to 0.835 and for two different levels of Reynolds number are shown in Figure 21. In high Reynolds number testing, $(C_L/C_D)_{max}$'s of 40 to 50 show higher values than those of low Reynolds number testing.

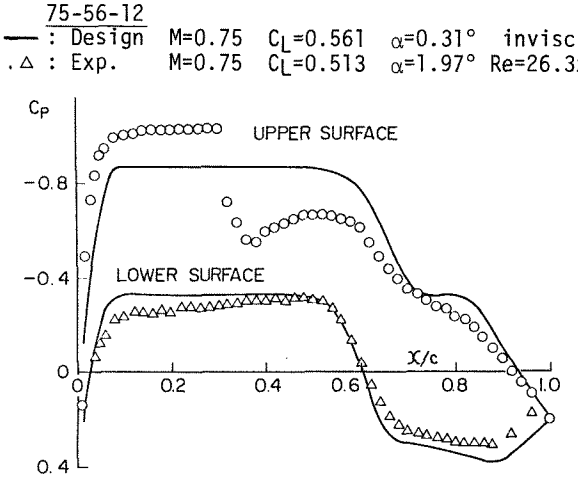

Figure 20. Pressure distributions of NAL 75-56-12 wing section.

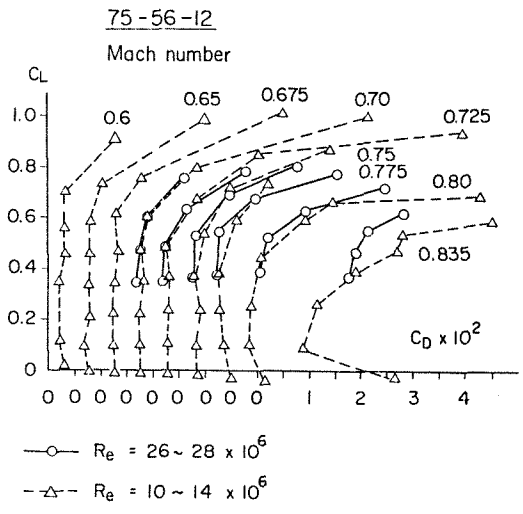

Figure 21. Polar curves of NAL 75-56-12 wing section.

5. Reynolds number effects

NACA 0012.

Reynolds number effects at high subsonic Mach numbers were investigated for the NACA 0012 wing section at M=0.6 to 0.8 and α=0° to 4°. Test conditions are shown in Table 1. The ratio of maximum to minimum Reynolds number is 6. In Table 1, A, B, C and D indicate the type of pressure distributions, which are subcritical, nearly shockless slightly supercritical, supercritical, and strong shock wave behind with a fairly large separation region, respectively.

Mach number	Reynolds number (10^6)	Angles of attack (deg.) 0	1	2	3	3.5	4	5	6	7
0.60	5.7 - 35	A	A	A	A	-	B	C	C	C
0.70	6.4 - 38	A	A	B	C	C	C	-	-	-
0.75	6.6 - 42	B	B	C	C	-	D	-	-	-
0.80	6.8 - 42	C	C	C	D	-	D	-	-	-

Table 1. Test conditions of the NACA 0012 wing section.

Pressure distributions.

For the pressure distributions of the A and B type, the Reynolds number effects are similar to the experiments until have been showing. For instance, the resulting C_D decreases and C_L/C_D increases with Reynolds number increase.

For supercritical conditions, examples of Reynolds number effects on pressure distributions at M=0.75, α=3°, M=0.8, α=0° and M=0.75, α=4° are shown in Figure 22(a), (b) and (c), respectively. The shock wave position on the upper surface moves rearward with increasing Reynolds number for all Mach numbers which were tested, as shown in Figure 22. Collected movements of the shock wave position are shown in Figure 23. At M=0.70 and M=0.75, the movements are small, however, at M=0.80, these become as big as 10% of chord length with Reynolds number increase. The rate of the shock wave movement to the Reynolds number change is high in the Reynolds number range from six million to twenty million at M=0.80. At the other range, movement is nearly frozen.

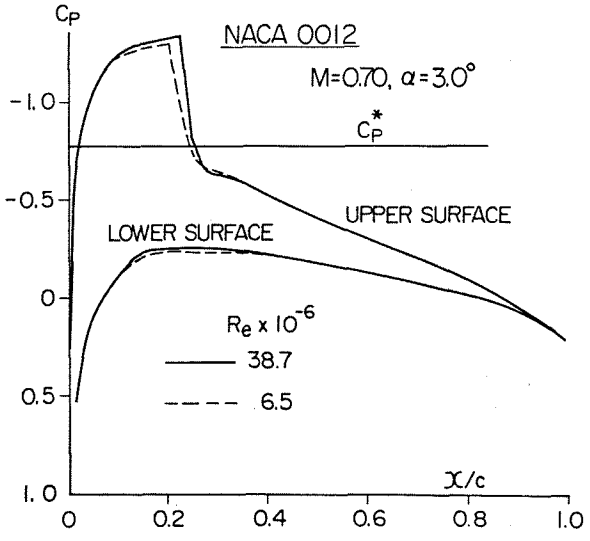

(a) Pressure distributions of type C.

Figure 22. Reynolds number effects on pressure distributions.

Aerodynamic coefficients.

The polar curves for minimum and maximum Reynolds numbers are shown in Figure 24. At M=0.60, M=0.70 and M=0.75, the polar curves approach the axis of C_L with decreasing minimum drag level, then, C_L/C_D is improved with the Reynolds number increase. However, at M=0.80, the counter situation occurs. The polar curve moves to the axis of C_D with increase of the minimum drag level when the Reynolds number increases. In the meaning of C_L/C_D, the performance of this wing section becomes worse as the Reynolds number increases. This situation is also observed in the cases of the wing section 777-626-13 as mentioned in Section 4. A symptom of this phenomenon was observed for 75-56-12 wing section. Namely, at high subsonic Mach numbers, say M=0.8, the lift to drag ratio C_L/C_D decreases and minimum drag level increases as the Reynolds number increases.

Pitching moment coefficients are shown in Figure 25. At high subsonic Mach numbers, high Reynolds number test results show a large nose-down pitching moment due to the rearward movement of the shock wave contrary to Figure 13.

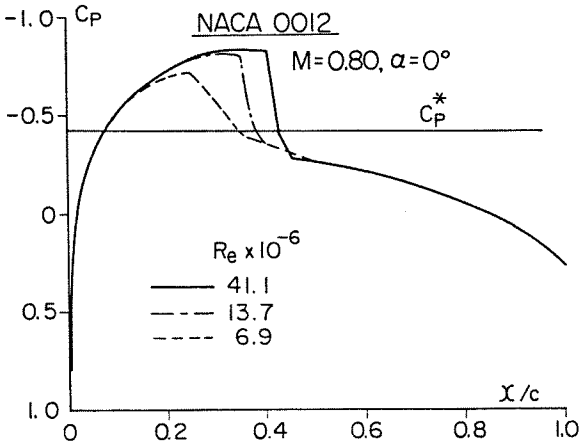

(b) Pressure distributions of type C.

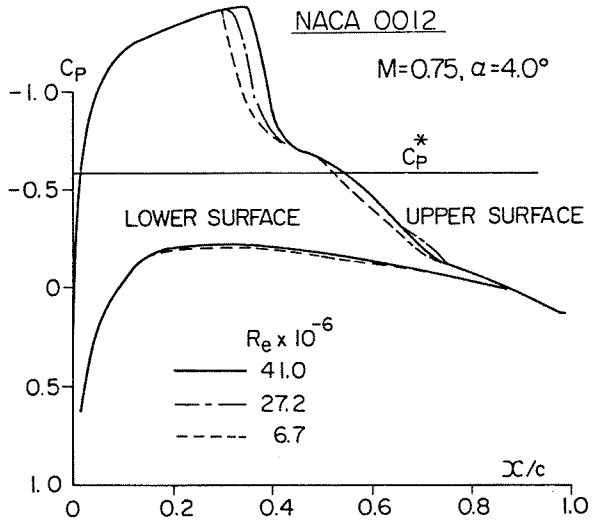

(c) Pressure distributions of type D.

Figure 22. Concluded.

6. Conclusion

A high Reynolds number two-dimensional transonic wind tunnel has been constructed and operated over a Mach number range of 0.2 to 1.15 and over a Reynolds number range of 4 million to 40 million.

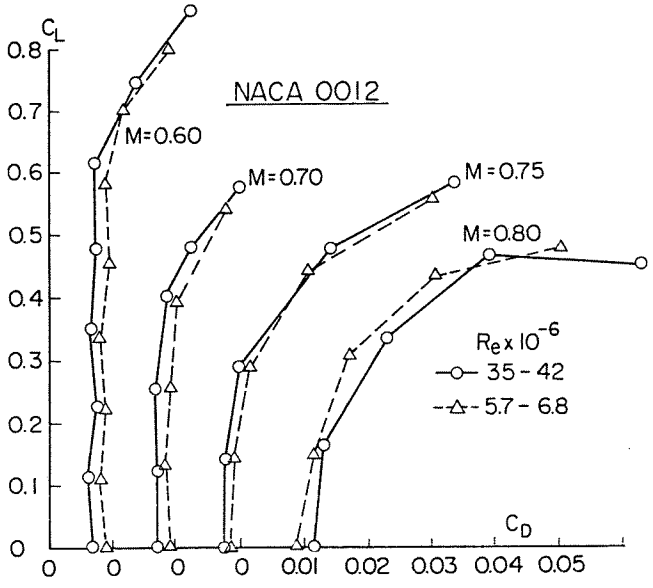

Figure 24. Polar curves of the NACA 0012 wing section.

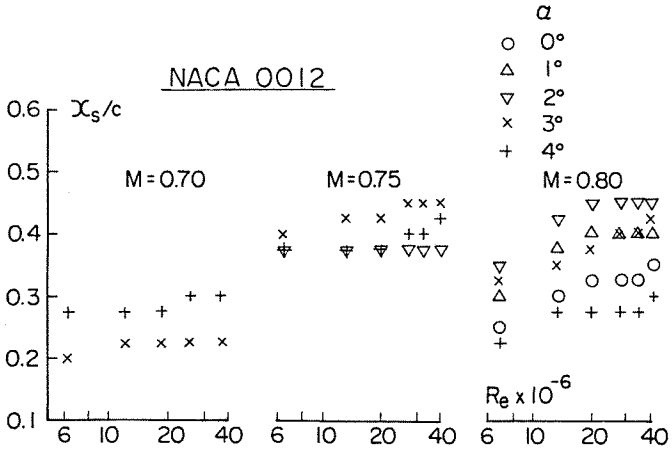

Figure 23. Reynolds number effects on shock wave position of upper surface.

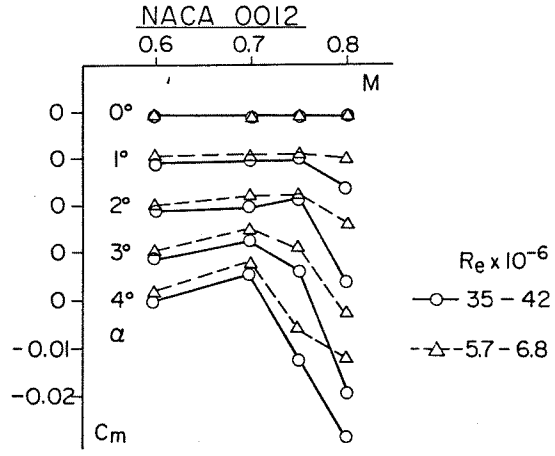

Figure 25. Pitching moments of the NACA 0012 wing section.

Results of the initial calibration are considered to have satisfied our expectation. The wind tunnel is successfully being used to investigate the characteristics of newly developed transonic airfoils at high Reynolds number in transonic regime. Reynolds number effects on airfoil characteristics are expected to make clear experimentally.

Acknowledgment

The author wishes to express his appreciation to Prof. T. Shigemi, Mr. K. Hirooka and Dr. H. Endo for their great contributions to constructing the wind tunnel. He would like to also acknowledge Messrs. S. Sakakibara, H. Miwa, Y. Oguni, M. Sato and H. Kanda for their cooperation in the wind tunnel testing.

References

1. Pearcey, H. H.; The Aerodynamic Design of Section Shapes for Swept Wings, Advances in Aero. Sci., Vol. 3, Pergamon Press, London (1962).

2. Nieuwland, G. Y.; Theoretical Design of Shock--Free Transonic Flow around Airfoil Sections, Aerospace Proceedings 66, Macmillan, London (1967).

3. Garabedian, P. R. and Korn, D. G.; Numerical Design of Transonic Airfoils, Numerical Solution of Partial Differential Equations II, Academic Press, New York (1971).

4. Whitcomb, R. T.; Review of NASA Supercritical Airfoils, ICAS Paper No. 74-10 (1974).

5. Jones, J. L.; Problems of Flow Simulation in Wind Tunnels, AIAA Paper No. 69-660 (1969).

6. Loving, D. L.; Wind Tunnel-Flight Correlation of Shock Induced Separated Flow, NASA TN D-3580 (1966).

7. Ludwieg, H. et al.; Problems of Wind Tunnel Design and Testing, AGARD Rep. No. 600 (1972).

8. Baals, D. D. (ed.); High Reynolds Number Research, NASA CP-2009 (1977).

9. Ohman, L. H. and Brown, D.; The NAE High Reynolds Number 15in. x 60in. Two-Dimensional Test Facility, NAE LTR-HA-4 (1970).

10. Pounds, G. A.; An Initial Two-Dimensional Wall Interference Investigation in a Transonic Wind Tunnel with Variable Porosity Test Section Walls, AIAA Paper No. 72-1011 (1972).

11. The Staff of the Second Aerodynamics Division; Construction and Performance of NAL Two--Dimensional Transonic Wind Tunnel, NAL TR--647T (1982).

12. Endo, H.; On the NAL Transonic Variable Density Windtunnel for Two-Dimensional Testing, Jour. Japan Soc. Aero. Space Sci. Vol. 26, No. 299 (1978) (in Japanese).

13. Sakakibara, S. and Baba, S.; Investigation of the Components of the NAL High Reynolds Number Two-Dimensional Wind Tunnel, Part I, NAL TR-465 (1976) (in Japanese).

14. Thwaites, B.; On the Design of Contractions for Wind Tunnels, R. & M. No. 2278 (1946).

15. Endo, H. et al.; Investigation of the Components of the NAL High Reynolds Number Two--Dimensional Wind Tunnel, Part II, NAL TR--476 (1976) (in Japanese).

16. Sakakibara, S. et al.; Investigation of the Components of the NAL High Reynolds Number Two-Dimensional Wind Tunnel, Part IV, NAL TR-606 (1980) (in Japanese).

17. Miwa, H.; Investigation of the Components of the NAL High Reynolds Number Two-Dimensional Wind Tunnel, Part III, NAL TR-597 (1980) (in Japanese).

18. Reed, T. D. et al.; Calibration of Transonic and Supersonic Wind Tunnels, NASA CR-2920 (1977).

19. Hartzuiker, J. P. et al.; On the Flow Quality Necessary for the Large European High-Reynolds Number Transonic Wind Tunnel LEHRT, AGARD-R-644 (1976).

20. Bauer, F. et al.; Supercritical Wing Sections II, Lecture Notes Eco. Math. Sys. Vol. 108, Springer Verlag (1975).

21. Stivers, L. S.; Effects of Subsonic Mach Number on the Forces and Pressure Distributions on Four NACA 64A-Series Airfoil Sections at Angles of Attack as High as 28°, NACA TN 3162 (1954).

22. Working Group 04; Experimental Data Base for Computer Program Assessment, AGARD AR-138 (1979).

23. Pindzola, M. and Lo, C. F.; Boundary Interference at Subsonic Speeds in Wind Tunnels with Ventilated Walls, AEDC TR 69-47 (1969).

24. Takashima, K. et al.;NAL TR to be published.

25. Shigemi, T.; A Contribution to the Analytical Hodograph Method for Shock-Free Transonic Airfoil Sections, Trans. Japan Soc. Aero. Space Sci. Vol. 24, No. 65 (1981).

26. Kamiya, N. et al.; Design and Test of Transonic Airfoils Under Consideration of Drag Divergence Mach Number AIAA Paper No. 78-1221 (1978).

27. Kamiya, N. and Hirose, N.; Research on Transonic Wings at the National Aerospace Laboratory Japan, ICAS-80-11.1 (1980).

28. Tranen, T. L.; A Rapid Computer Aided Transonic Airfoil Design Method, AIAA Paper No. 74-501 (1974).

29. Ishiguro, T. et al.; Transonic Airfoil Design of Full Potential Flow, NAL TR-672 and TR--673 (1981) (in Japanese).